A comparison of nanoindentation and mesoscale measurements on polychloroprene (Neoprene) rubber

by

Mohammad Ansarin

A Thesis Submitted to the

Graduate School of Sciences and Engineering

in Partial Fulfillment of the Requirements for

the Degree of

Master of Science

in

Biomedical Sciences and Engineering

Koc University

May 2015

Koc University

Graduate School of Sciences and Engineering

This is to certify that I have examined this copy of a master's thesis by

Mohammad Ansarin

and have found that it is complete and satisfactory in all respects,

and that any and all revisions required by the final

examining committee have been made.

Committee Members:

_____

Cagatay Basdogan, Ph. D. (Advisor)

_____

Murat Sozer, Ph. D.

_____

Gunay Anlas, Ph. D.

Date: _____

ABSTRACT

Nanoindentation has risen in popularity as an alternative approach to mesoscale measurements for characterizing material properties. However, many of the difficulties inherent to the measurement and characterization of viscoelastic materials at nanoscale have not been yet solved. In this research, we compare nanoindentation and mesoscale measurements performed on polychloroprene rubber and attempt to better understand the observed differences. We conducted nanoindentation creep experiments using Berkovich and flat punch tips. Our mesoscale measurements consisted of normal compression, tension, and relaxation, and a Shore-A hardness test. We fit a 5-parameter Generalized Maxwell model to the normal relaxation data and a corresponding Kelvin-Voigt model to the creep data. We observed that nanoscale measurements returned higher elastic modulus values than mesoscale measurements. Hence, the surface material properties of the polychloroprene specimens are different than their bulk material properties. However, it is important to emphasize that differences in the measurement devices, measurement methods, and modeling assumptions may have contributed to the discrepancies in the results.

ÖZET

Nanoindentasyon, materyal özelliklerinin nitelendirilmesi için kullanılan orta ölçekli yöntemlere alternatif olarak yaygınlık kazanan bir yöntemdir. Ancak, viskoelastik maddelerin nano boyutta nitelendirilme ve ölçülmesinde yaşanan zorluklar, hala çözülememiştir. Bu araştırmada, polikloropren lastik üzerinde nanoindentasyon ve orta ölçekli yöntemlerle elde edilen ölçümler karşılaştırılarak, bu iki yöntem hakkında geniş kapsamlı bilgi edinilmesi hedeflenmiştir. Bu sebeple, çalışmada Berkovich ve düz delgi uçları kullanılarak nanoindentasyon yöntemi ile sürünme deneyleri yapılmıştır. Orta ölçekli yöntemlerle yapılmış ölçümler; normal sıkıştırma, germe, gevşeme ve Shore-A sertlik testlerinden oluşmaktadır. Normal gevşeme verileri, 5-parametrelik bir Generalized Maxwell modeline; sürünme verileri ise 5-parametrelik bir Kelvin-Voigt modeline yakınsanmıştır. Nano ölçekte elde edilen ölçümlerin, orta ölçek yöntemiyle elde edilen ölçümlere göre çok daha yüksek elastik modül değerlerine sahip oldukları gözlemlenmiştir. Böylece, polikloropren örneklerinin yüzey maddesel özelliklerinin, iç özelliklerinden farklı olduğu sonucuna varılmıştır. Ancak, ölçüm cihazları, ölçüm yöntemleri ve modelleme varsayımlarının aralarındaki farklılıkların, sonuçlardaki tutarsızlığa katkı sağlamış olabilecekleri unutulmamalıdır.

ACKNOWLEDGEMENTS

I thank Professor Cagatay Basdogan, the Robotics and Mechatronics Laboratory members and alumni, the Koc University community, and my family for their support during my studies. I also thank our partners in the MeProVisc project for their input.

I am grateful for Koc University's Graduate School of Sciences and Engineering, the Scientific and Technological Research Council of Turkey (TUBITAK), and the European Association of National Metrology Institutes (EURAMET) for providing resources and information in various parts of the course of my master's degree research.

TABLE OF CONTENTS

Abstract III
Özet IV
Acknowledgements V
List of Tables VII
List of Figures VIII
Nomenclature X
Introduction 1
Materials and Methods 5
2.1. Nanoindentation 5
2.1.1. Berkovich Tip 5
2.1.2. Flat-punch 8
2.2. Mesoscale Measurements 10
2.2.1. Shore hardness 10
2.2.2. Normal compression 10
2.2.3. Normal relaxation 12
2.2.3.1. Relaxation Model 13
2.2.4. Tensile Test 15
Experimental Results 17
3.1. Nanoindentation Creep 17
3.1.1. Berkovich Tip 17
3.1.2. Flat Punch Tip 19
3.2. Mesoscale Measurements 19
3.2.1. Shore hardness 19
3.2.2. Normal compression 19
3.2.3. Normal relaxation 21
3.2.4. Tensile Test 23
Discussion 24
4.1. Discussion of current results 24
4.1.1. Departure from continuum mechanics 26
4.1.2. Data scatter in nanoindentation 28
4.2. Comparison of nanoindentation results with those of earlier indentation studies 29
Conclusions 31
Bibliography 32
Appendix A 37

LIST OF TABLES

Table 1 – Overview of all measurements 16

LIST OF FIGURES

Figure 1 - a) Force-displacement profile for nanoindentation creep (P_{max} = 0.2 mN, t_{load} = 3 s, t_{hold} = 3000 s); b) Material response in time _____6

Figure 2 - Normal compression and relaxation experimental setup. _____11

Figure 3 – Computer analysis of the shape factor effect. _____11

Figure 4 – Generalized Maxwell Model. _____13

Figure 5 - Tensile elongation experimental setup. _____15

Figure 6 - Sample Berkovich indentation creep curve fit (t_{hold} = 3000s).____18

Figure 7 – The results of the creep experiments performed with the Berkovich indenter.___18

Figure 8 – Stress-strain curves for cycle 1 (dashed line) and cycles 10 - 17 (solid lines) of the Neoprene (boxed section magnified).____20

Figure 9 - Elastic modulus versus strain for loading rates of 0.08 mms^{-1} (dashed line), 0.16 mms^{-1} (solid line), and 0.32 mms^{-1} (dash-dotted line).____20

Figure 10- Comparison of different Maxwell model sizes in fitting relaxation data. Regression values are written above curves.____21

Figure 11 – The change in relaxation modulus as a function of time for normal strains of 5% (green), 10% (red), and 15% (blue).____22

Figure 12 – Results of the tensile test. _____23

Figure 13 – Summary of results of all experiments performed at nano and meso scales. ___26

Figure 14 – Optical microscope (left, 5x) and scanning electron microscope (right, 5000x) images of one polychloroprene (Neoprene) sample. _____29

Figure 15 – Comparison of modulus values reported for Neoprene rubber in our nanoindentation experiments with those of earlier studies. _____30

Figure 16- Modulus versus time for one Maxwell arm under ramp-and-hold loading. Varying E shows a scaling of the curve (left), while increasing τ pushes the curve rightward (right). 38

Figure 17 - Modulus versus time for model fit and parameter variations on first Maxwell arm (smaller τ). _____39

Figure 18 - Modulus versus time for model fit and parameter variations on second Maxwell arm (larger τ). _____40

Figure 19 - Modulus versus time for model fit and parameter variations on steady-state response coefficient. _____40

Figure 20 - R^2 value versus deviation for each model coefficient (with other coefficients held constant). The deviation percentage shows variations in each coefficient. _____41

NOMENCLATURE

k	Rate of force loading
P	Force
t	Time
t_0	Loading time
t_{end}	End of holding time / unloading time
P_{max}	Holding force
h	Displacement in indentation
E^*	Indentation modulus
ψ	Included half-angle of indenter tip
γ	Contact-to-total depth constant
E_i^*, θ_i	Kelvin-Voigt model coefficients
σ	Normal stress
ε	Normal strain
ξ	Elastic modulus in Laplace domain
$\bar{\sigma}$, $\bar{\varepsilon}$	Stress and strain in Laplace domain
E	Elastic modulus
E_0,E_∞	Instantaneous, steady state elastic modulus
ν	Poisson's ratio
R	Flat punch indenter radius
A	Shore-A hardness
R_d	Shore-A hardness durometer tip radius
S	Shape factor
r	Radius of cylindrical samples
d	Thickness of cylindrical samples
E_i, η_i, τ_i	Maxwell model coefficients
E_{rel}	Relaxation modulus
$\Delta\sigma$	Incremental stress
$\Delta\varepsilon$	Incremental strain
F	Tensile force
A	Surface area
l_0	Initial length
Δl	Deformation

Chapter 1

INTRODUCTION

Nanoindentation is a new technique for probing the mechanical properties of a material. It is increasingly used to investigate the mechanical behavior of biological materials ([1–4]), composites ([5]), and thin films ([6–9]). However, many factors affect the outcome of the nanoindentation measurements ([10]). These factors include the measurement devices and protocols, indenter type, modeling assumptions, the choice of sample material ([11,12]), and environmental conditions such as temperature and humidity ([13]).

In nanoindentation, since a small probe penetrates into the large surface of test specimens, some modeling assumptions are necessary to estimate the material properties [11]. These assumptions would be different, sometimes contradictory to previous assumptions in the mesoscale. The test specimen's properties also affect nanoscale indentation measurements differently from mesoscale measurements [14]. Also, a delicate control of temperature and humidity is necessary in nanoindentation measurements while the mesoscale measurements are relatively less sensitive to these parameters [13]. These factors can further cause discrepancies between nanoindentation and conventional mesoscale measurements, and also between different nanoindentation techniques. By choosing a suitable sample material, making valid modeling assumptions, and keeping environmental conditions steady, we investigate the effect of nanoindentation devices and protocols and also indenter types on the mechanical property results of a sample soft material; we also investigate the validity of our modeling assumptions, based on the observed discrepancies.

Indentation has previously been used extensively in probing the mechanical properties of various materials, mostly based on the classical Hertzian [15] model of contact, further

analyzed by Sneddon [16]. Oliver and Pharr [17] extended this analysis to micro- and nanoscale measurements. These analyses and their assumptions, along with subsequently developed measurement techniques have later been researched to find an optimal method for indenting each material; a method which leads to a reliable set of characteristic mechanical properties.

A series of these works are devoted to understanding how accurately nanoindentation experiments replicate the results of broadly accepted conventional measurement tests. Researchers have obtained mixed results in this domain, especially in the characterization of viscoelastic materials. For example, Mazeran et al. [18] developed a new viscoelastic-plastic model to fit results from their Berkovich indenter creep, quasi-static indentation, and conventional tensile experiments, with all three results agreeing fairly well for 3 different polymers. Herbert et al. [13] compared flat punch nanoindenter results to mesoscale dynamic mechanical analysis (DMA) and creep measurements and observed agreement between the results. Monclus and Jennett [19] also have conducted DMA using conventional and Berkovich tip indentation methods, finding synonymous results. Kaufman et al.'s [20] experiments, consisting of spherical tip nanoindentation and normal compression, also resulted in agreeable modulus values. However, Champhekar [11] measured the storage and loss moduli of PDMS samples 2-3 times higher in nanoindentation than in conventional DMA. Carrillo et al. [21] also measured the material properties of PDMS samples using unconfined compression and quasi-static nanoindentation. They used both Oliver and Pharr's [17] and Hertz's [15] [22] model to fit the data, yet obtained modulus values significantly higher than those of the mesoscale compression experiments. They attributed this discrepancy to adhesion effects, but expressed that extra insight into nanoscale contact mechanics is required to fully understand the underlying phenomena. This pattern also continues in other works, where results from nanoindentation methods show signs of measurement bias and necessitate subsequent investigation ([9,12]).

There is also debate in the community as to which indenter tip provides the most reliable results in nanoindentation. Each indenter tip and measurement method has individual advantages and disadvantages, with each contributing to discrepancies between its results and corresponding mesoscale measurements. Recently, flat-punch nanoindenter tips have gained popularity due to some geometrical advantages over pyramidal-conical (e.g. Berkovich) and spherical tips ([13]). In flat punch indentation, shear deformation regions are remote from the hydrostatic zone beneath the indenter punch, allowing simpler stress tensor assumptions. Flat punch indenters are also immune to transient behavior and thermal drift ([13]). Cheng et al. [23] argue that the flat-punch indenters also have fewer problems during initial contact compared to the pyramidal-conical indenters typically used in commercial nanoindentation systems. However, flat-punches tend to introduce heterogeneous stress, with higher concentrations on the punch's periphery; a significant amount of heterogeneity may invalidate linear viscoelasticity considerations. An investigation of these advantages and disadvantages would further elucidate its relative superiority or inferiority to other indentation tips.

Previously, little comparison has been done between flat punch and other indenter geometries in the characterization of viscoelastic materials. Wang et al. [24] have performed DMA and quasi-static indentations on PDMS using both Berkovich and flat punch tips. After accounting for each measurement's artifacts, they found similar modulus values. However, their flat-punch tip was 1002 µm in diameter, larger than usual nanoindentation flat-punch tips. An appropriate comparison between results obtained from nanoindentation experiments with flat-punches and other geometries and corresponding mesoscale tests can help us further understand the utilities and setbacks of each method.

In this work, we performed an array of nanoscale and conventional mesoscale measurements on polychloroprene rubber samples and discuss the possible factors affecting discrepancies between the measurements. We initially explain the modeling and experimental procedures

utilized for this investigation (Chapter 2). In Chapter 3, we report the elastic modulus of polychloroprene rubber as estimated by the nanoindentation creep experiments performed with Berkovich and flat-punch tips and those obtained by conventional mesoscale experiments: normal compression, normal relaxation, simple tension, and the Shore-A hardness test. Afterwards, we further compare our results between each other and with previously reported mechanical property results for polychloroprene (Neoprene) rubber (Chapter 4). We also examine discrepancies between the results and review our modeling considerations. We believe this research endeavor to be the first comparison of the time-dependent mechanical properties of polychloroprene rubber in the meso- and nanoscale.

Chapter 2

MATERIALS AND METHODS

We performed 2 nanoindentation and 4 conventional mesoscale experiments to characterize the material properties of polychloroprene rubber samples. The experiments performed at the mesoscale were a) normal compression, b) normal compressive relaxation, c) simple tensile test, and d) Shore-A hardness test. Two creep indentation experiments were performed independently at the nanoscale using Berkovich and flat punch tips.

We chose Polychloroprene (Neoprene) rubber for the experiments due to its viscoelastic characteristics. In addition, it showed negligible plastic deformation in our preliminary experiments. The material is also resistant to abrasion and temperature fluctuations. Our choice of material also facilitated the Shore-A hardness test, whose hardness result can be converted into elastic modulus [25]. Furthermore, earlier studies performed by Lim and Chaudhri ([12,26]) and others ([11]) have shown that polychloroprene rubber is a good candidate for performing nanoindentation experiments. The samples used in our experiments were extracted from 3.2 and 6.4 mm thick sheets, acquired from Grainger Inc. The size and shape of the samples varied depending on the requirements of each setup and experiment.

2.1. Nanoindentation

2.1.1. Berkovich Tip

We used a UNHT (Ultra Nanoindentation Tester, Anton Paar Tritec) with a Berkovich tip (detailed in [27] and [19]) to perform nanoindentation creep experiments on 10*10 mm^2 square samples of 3.2 mm thickness. The Berkovich tip is a three-faced pyramid tip, with an axisymmetric equivalent opening angle of 140.6° and a half-included angle of 65.35°. The tip's ending is spherical with a radius of 200 nm. We mounted and secured the samples on a stage

using superglue. After mounting, we conducted measurements in three stages (Figure 1): first, we lowered the indenter with a maximum force of 0.2 mN onto the sample in 1, 3, or 10 seconds (loading time). The indenter was held at this force for various holding times ranging from 10 to 3000 seconds. Afterwards, the force was unloaded in 10 seconds. We repeated each measurement 10 to 17 times at different locations on the sample (Table 1). The output of this experimental procedure, known as a ramp-hold indentation test, is the time-displacement curve (Figure 1, right). We varied loading and holding times to observe the effect of these values on the measured material parameters. All experiments were conducted in a controlled lab environment with a temperature of 23.6 ±0.1℃ and a relative humidity of 40%.

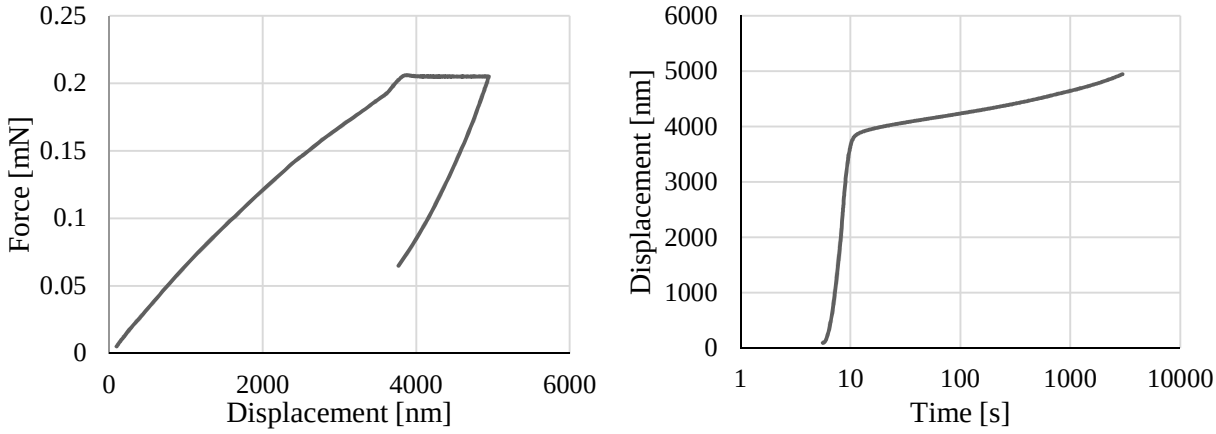

Figure 1 - a) Force-displacement profile for nanoindentation creep (P_{max} = 0.2 mN, t_{load} = 3 s, t_{hold} = 3000 s); b) Material response in time

We used viscoelastic correspondence analysis based on the Boltzmann superposition principle from continuum mechanics to calculate the indentation moduli from the experimental creep data ([28]). In the loading segment, the rate of force, k = dP/dt, was constant, where *P* is the force applied to the sample. Consequently, the time (t_0) for the applied force to reach its holding value (P_{max}) has an inverse relation with the rate ($t_0 k = P_{max}$). During the holding segment ($t_0 < t < t_{end}$), the force was constant.

In conical-pyramidal indenters such as the Berkovich indenter, the material's displacement (*h*) under load (*P*) is given as ([29])

$$h^2(t) = \frac{2\gamma^2}{\pi tan\psi}\frac{P}{E^*} \qquad \textit{Equation 1}$$

where E^* is the indentation modulus, ψ is the indenter's included half-angle (65.35 degrees for Berkovich tip), γ is a constant relating contact depth to total depth and is taken as unity for polymeric materials [19].

Since polychloroprene is viscoelastic, $1/E^*$ would be time-dependent and we can replace it with a creep compliance integral. During indentation, each force increment initiates creep as it is applied. If t is current time and u is the time at which an increment of force was applied, the amount of displacement creep that has occurred at each point in time t can be formulated as

$$h^2(t) = \frac{2}{\pi tan\psi}\int_0^t J(t-u)\frac{dP(u)}{du}du = \frac{2}{\pi tan\psi}\, I\,. \qquad \textit{Equation 2}$$

To solve the integral I, we model the creep compliance function with a 2-element (i.e. 2-arm) Kelvin-Voigt representation, which can be written as

$$J(t) = \frac{1}{E_0^*} + \frac{1}{E_1^*}\left[1 - e^{\left(\frac{-t}{\theta_1}\right)}\right] + \frac{1}{E_2^*}\left[1 - e^{\left(\frac{-t}{\theta_2}\right)}\right] \qquad \textit{Equation 3}$$

where E_0^* is the instantaneous indentation modulus and E_i^* and θ_i represent the indentation modulus and time constant of each element (arm), respectively. The creep compliance function, *J(t)*, is the sum of the instantaneous creep response and the creep responses of each arm (the contribution of each arm is initially zero at t=0 and increases to $1/E_i^*$ as t→∞). There is a tradeoff in selecting the number of arms used in the model. With a higher number of arms, the uniqueness of the material coefficients is questionable; with fewer arms, the model may not be able to fit the data adequately. We observed that the 2-arm model provides a good balance.

Now, by substituting *J(t)* into *I*, we can evaluate the integral (at $t > t_0$) as

$$I = k\left(\frac{t_0}{E_0^*} + \frac{t_0}{E_1^*} + \frac{t_0}{E_2^*}\right) - k\left(\frac{\theta_1}{E_1^*}\right)\left(e^{\frac{t_0}{\theta_1}} - 1\right)e^{\frac{-t}{\theta_1}} - \left(\frac{\theta_2}{E_2^*}\right)\left(e^{\frac{t_0}{\theta_2}} - 1\right)e^{\frac{-t}{\theta_2}}. \quad \textit{Equation 4}$$

Substituting this into the displacement equation, we find:

$$h^2(t) = \frac{2k}{\pi tan\psi}\left\{\left(\frac{t_0}{E_0^*} + \frac{t_0}{E_1^*} + \frac{t_0}{E_2^*}\right) - \left(\frac{\theta_1}{E_1^*}\right)\left(e^{\frac{t_0}{\theta_1}} - 1\right)e^{\frac{-t}{\theta_1}} - \left(\frac{\theta_2}{E_2^*}\right)\left(e^{\frac{t_0}{\theta_2}} - 1\right)e^{\frac{-t}{\theta_2}}\right\}. \quad \textit{Equation 5}$$

This equation was used to fit the experimental creep data to estimate E_i^* and θ_i. Although creep compliance and stiffness moduli do not have a general direct reciprocal relationship, they do so for the end points of the time domain [30]. After estimating the instantaneous and steady-state elastic indentation moduli from the experimental data via curve-fitting, we can obtain the instantaneous (E_0) and steady-state (E_∞) elastic moduli using the following relations:

$$\frac{1}{E_\infty^*} = \frac{1}{E_0^*} + \sum \frac{1}{E_i^*}\ and \quad \textit{Equation 6}$$

$$\begin{cases} E_0 = (1 - \nu^2)E_0^* \\ E_\infty = (1 - \nu^2)E_\infty^* \end{cases} \quad \textit{Equation 7}$$

where ν is the Poisson' ratio and is taken as $\nu = 0.5$.

2.1.2. Flat-punch

We performed nanoindentation creep experiments with a cylindrical flat tip indenter having a diameter of 4.75 µm on 10*10*3.175 mm Neoprene samples. These samples were mounted and secured onto a custom-built tilt stage using superglue. For this indentation experiment, we used a UMIS (Ultra Micro-Indentation System)-2000 nanoindenter (SCIRO, Lindfield, Australia) with IBIS control software (Fischer-Cripps, Australia). Force and displacement detection was based on linear variable differential transformers (LVDT), with resolutions of 0.2 µN and 1 nm, respectively. We controlled the environment's temperature and humidity levels, stabilizing them between 25-25.2 ℃ and 46-48%, respectively. Thermal and electronic drift were insignificant over the time scale of the flat-punch indentation experiments.

As previously discussed in the introduction, two challenges exist in using a flat-tip cylindrical indenter. The first, stress concentration around the perimeter of the tip, was overcome by slightly rounding the edges during the manufacturing process of the indenter. The second problem of proper surface alignment was resolved by building a tilt stage to accurately align the sample and the indenter surfaces. We determined the tilting angle by analyzing atomic force microscopy (AFM) images of the indentation footprints.

We conducted 10 nanoindentation creep experiments by indenting the material in 20 force increments up to a maximum hold force of 0.2 mN. The procedure was similar to the Berkovich indentation creep experiment. This loading procedure took approximately 5s, after which we held the indenter at the maximum force for 130s before unloading.

For the flat tip cylindrical indenter, the relation between displacement (h) and load (P) is given as [29]

$$h = \frac{1}{2R}\frac{P}{E^*} \qquad \textit{Equation 8}$$

where R is the indenter radius. Replacing $1/E^*$ with a viscoelastic integral operator for creep gives the Boltzmann integral equation

$$h(t) = \frac{1}{2R}\int_0^t J(t-u)\frac{dP(u)}{du}\,du. \qquad \textit{Equation 9}$$

If we again use a 2-arm Kelvin-Voigt model for the creep function, we obtain the following equation:

$$h(t) = \frac{k}{2R}\left\{\left(\frac{t_0}{E_0^*}+\frac{t_0}{E_1^*}+\frac{t_0}{E_2^*}\right)-\left(\frac{\theta_1}{E_1^*}\right)\left(e^{\frac{t_0}{\theta_1}}-1\right)e^{\frac{-t}{\theta_1}} - \left(\frac{\theta_2}{E_2^*}\right)\left(e^{\frac{t_0}{\theta_2}}-1\right)e^{\frac{-t}{\theta_2}}\right\}. \qquad \textit{Equation 10}$$

As before, the indentation moduli and time constants were estimated via curve fitting this model to the experimental creep data, after which we can obtain the instantaneous and steady-state elastic modulus values using Equation 6 and Equation 7.

2.2. Mesoscale Measurements

2.2.1. Shore hardness

We used a shore-A hardness durometer (Shore Instrument & Mfg. Co., Inc., New York, USA) to measure the hardness of the rubber samples. The samples displayed an average of 53 shore-A hardness. Shore-A hardness values can be converted to elastic modulus using the following formula suggested by Kunz and Studer [25] for polymeric elastomers

$$E = \frac{1-\nu^2}{2R_d}\ \frac{0.549 + 0.07516S_A}{0.025(100 - S_A)}(2.6 - 0.02S_A) \qquad \textit{Equation 11}$$

where S_A is the Shore-A hardness and R_d is the tip radius of the durometer (0.395 mm).

2.2.2. Normal compression

We conducted compression experiments with rubber samples at mesoscale by following the experimental protocol given in ISO 7743:2008. The experiments were performed with a rheometer (Antor Paar GmbH, MCR102) at a temperature of 24℃ (Figure 2). The rheometer's force sensor in the normal direction has a resolution of 1 mN. We cut 15 mm diameter cylindrical samples from the 6.4 mm thick batch and compressed them up to 15% normal strain. In addition to the ISO's referenced strain loading rate of 0.16 mms^{-1}, we also used 0.08 and 0.32 mms^{-1} to understand what effect, if any, this velocity has on the results. The samples were pre-conditioned via cyclic loading to obtain consistent force-displacement data. We observed that the loading-unloading force curves reach a steady state after 10 cycles, but cycles were continued up to 17 to show convergence. The actual (apparent) elastic modulus was calculated after correcting for shape factor effects. The experiment was repeated with two samples each tested twice, and the mean values are reported here.

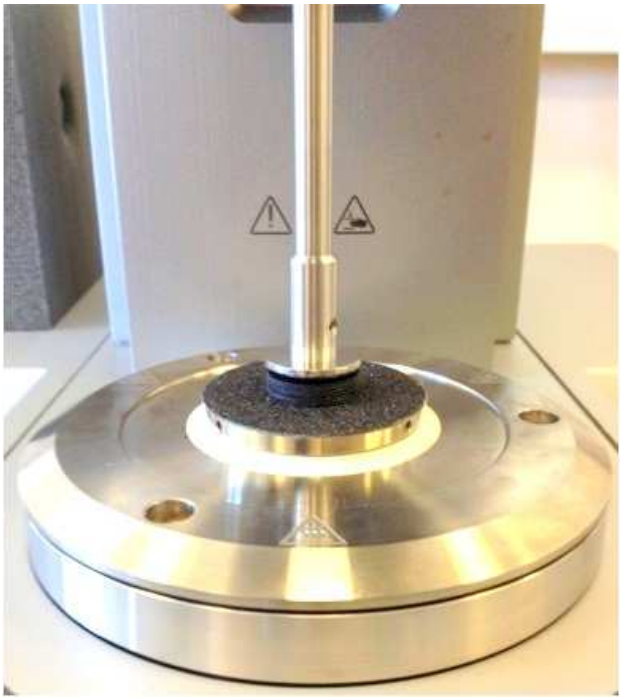

Figure 2 - Normal compression and relaxation experimental setup.

In our setup, sandpapers having a grain size of P80 are attached to the parallel plates of the rheometer using a double-sided tape (3M-9473PC) to ensure that no slippage occurs between the plates and the sample during the compression experiments. This procedure prevents the sample from dilating radially when normal strain is applied. As a result, additional shear stress forms in the center regions of the sample, adding to the normal stress and force response (Figure 3). This extra stress causes the compression elastic modulus to be overestimated from the measurements, for which the ISO 7743:2011 standard suggests corrections.

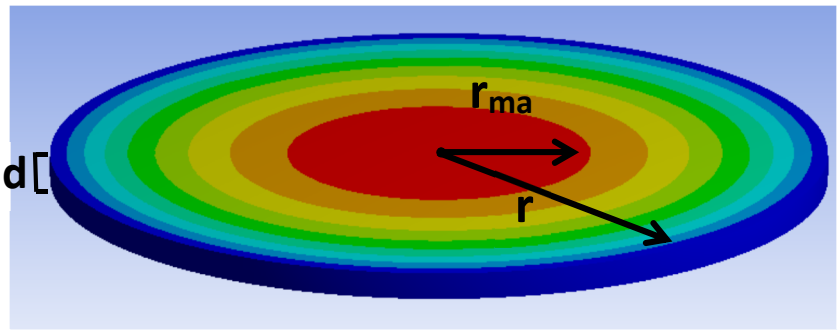

Figure 3 – Computer analysis of the shape factor effect.

The Young's modulus of cylindrical rubber discs can be corrected for shape factor effects based on the formula

$$E = \frac{\sigma}{\varepsilon}\left(\frac{1-\varepsilon}{1+2KS^2}\right) \qquad \textit{Equation 12}$$

where E is the Young's modulus and K is the correction factor. The normal stress (σ) and strain (ε) are obtained directly from the experimental measurements. The shape factor (S), which represents the ratio of the strained area to the non-strained area, is defined as

$$S = \frac{r}{2d} \qquad \textit{Equation 13}$$

where r and d are the radius and thickness of the cylindrical sample, respectively. It is evident that thinner and larger samples tend to have higher shape factors, which results in a higher elastic modulus. Lindley [31] tabulated the correction factor (K) for typical natural rubber vulcanizates, which we assume to be the same for our neoprene samples [32]. Hence, we can use Equation 12 to correct the measurements for shape factor effects.

2.2.3. Normal relaxation

We also investigated the rubber's dynamic material properties using force relaxation experiments performed in the normal direction. We conducted the experiments in accordance with ISO standard 3384-1 using the same rheometer detailed in Section 2.2.2. We prepared cylindrical samples of 13 mm diameter and 6.4 mm thickness. We set the loading velocity and holding time to 0.013 mms^{-1} and 1800 seconds, respectively. This experiment was repeated with three samples, each tested once with normal strains of 5%, 10%, and 15% as suggested in the ISO standard; the mean values are reported in this paper. We applied shape factor corrections to the relaxation data as in the case of compression experiments (Section 2.2.2).

2.2.3.1. Relaxation Model

We modeled the relaxation response of the neoprene using a generalized Maxwell model (Figure 4), previously detailed by Sedef [33]. This model is equivalent to the Kelvin-Voigt model used for processing the nanoindentation creep data.

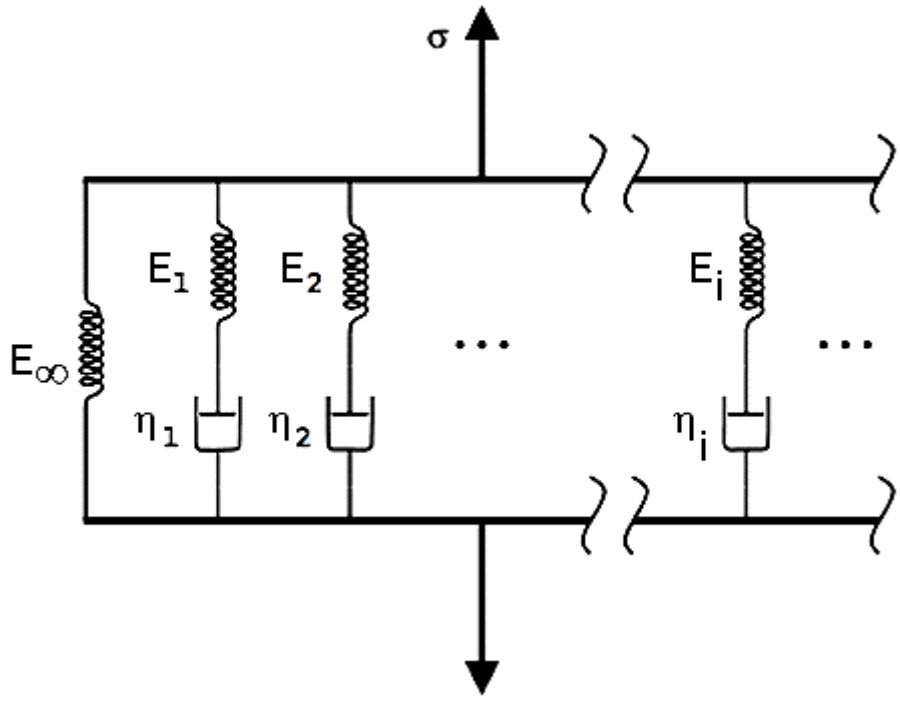

Figure 4 – Generalized Maxwell Model.

In this model, each spring-dashpot arm responds to strain as

$$E_i\dot{\varepsilon} = \dot{\sigma}_i + \frac{E_i\sigma_i}{\eta_i} \qquad \textit{Equation 14}$$

where η_i is the damping coefficient ($\eta_i = E_i\tau_i$, τ_i is the time constant of each arm). We can take our loading segment to be a constant ramp (i.e. $\dot{\varepsilon}$ is constant) and solve the equation by adding the response contributions from each arm. In the Laplacian domain, each contribution would be (i = 1, 2… n)

$$E_i\bar{\varepsilon}s = \bar{\sigma}_i s + \frac{\bar{\sigma}_i}{\tau_i} \qquad \textit{Equation 15}$$

which rearranges to

$$\bar{\sigma_i} = \frac{E_i s}{s + \frac{1}{\tau_i}} \bar{\varepsilon}. \qquad \textit{Equation 16}$$

Since in the Laplacian domain, we also have

$$\bar{\sigma} = \sum_{0}^{n} \bar{\sigma_i} = \xi \bar{\varepsilon} \qquad \textit{Equation 17}$$

where ξ is the modulus in the Laplacian domain, we can find this modulus as

$$\xi = E_\infty + \sum_{1}^{n} \frac{E_i s}{s + \frac{1}{\tau_i}}. \qquad \textit{Equation 18}$$

If we assume a ramp-and-hold input, take the reverse Laplace transform of this formula and input the initial conditions, we can obtain the relaxation elastic modulus for $t > t_0$ as

$$E_{rel}(t) = E_\infty - \sum_{1}^{n} \frac{E_i \tau_i}{t_0} \left(1 - e^{\frac{t_0}{\tau_i}}\right) e^{\frac{-t}{\tau_i}}. \qquad \textit{Equation 19}$$

In this formula, $\tau_i = \frac{\eta_i}{E_i}$ and t_0 is the loading time. We again found that for the force relaxation a minimum of 2 arms in the Generalized Maxwell model (i.e. 5 parameters) provides a suitable fit. We can use this model to obtain

$$E_{rel}(t) = E_\infty - \frac{E_1 \tau_1}{t_0} \left(1 - e^{\frac{t_0}{\tau_1}}\right) e^{\frac{-t}{\tau_1}} - \frac{E_2 \tau_2}{t_0} \left(1 - e^{\frac{t_0}{\tau_2}}\right) e^{\frac{-t}{\tau_2}}. \qquad \textit{Equation 20}$$

By curve-fitting this formula to the relaxation data, we estimate the viscoelastic material coefficients (E_i and τ_i). We also conducted a parametric study on our relaxation model, the details of which are articulated in Appendix A. The 5 material coefficients found in the curve fitting enable us to calculate the relaxation modulus at the end points of the time domain as

$$\begin{cases} t \to 0 : E(t) \to E_0 = E_\infty - \frac{E_1 \tau_1}{t_0} \left(1 - e^{\frac{t_0}{\tau_1}}\right) - \frac{E_2 \tau_2}{t_0} \left(1 - e^{\frac{t_0}{\tau_2}}\right). \\ t \to \infty : E(t) \to E_\infty \end{cases} \qquad \textit{Equation 21}$$

2.2.4. Tensile Test

We also independently performed tensile tests on the rubber specimens in a climate-controlled environment using a custom-made setup adhering to the ISO-527 standard (Figure 5). In this setup, “bone-shaped” neoprene samples are pulled while their force response is measured by a load cell with a force resolution of 5 mN. The environmental temperature during these experiments is 21.0 ±0.5℃. The bone-shaped samples are cut out of 6.4 mm thick Neoprene sheets, with the middle testing section having a width of 9.96 mm and length of 50 mm. The samples are pulled from 0 to 3.5 mm (0 to 18% normal tensile strain) at four different strain rates of 0.01, 0.03, 0.06, and 0.1 mms^{-1}. As the material is viscoelastic, the strain rate affects the force response. For this reason, we first calculated the elastic modulus at each strain rate by fitting a line to the stress-strain data in the linear region. Afterwards, we fitted a second order polynomial to the elastic modulus values at different strain rates and estimated the elastic modulus at zero strain rate from the curve-fit equation.

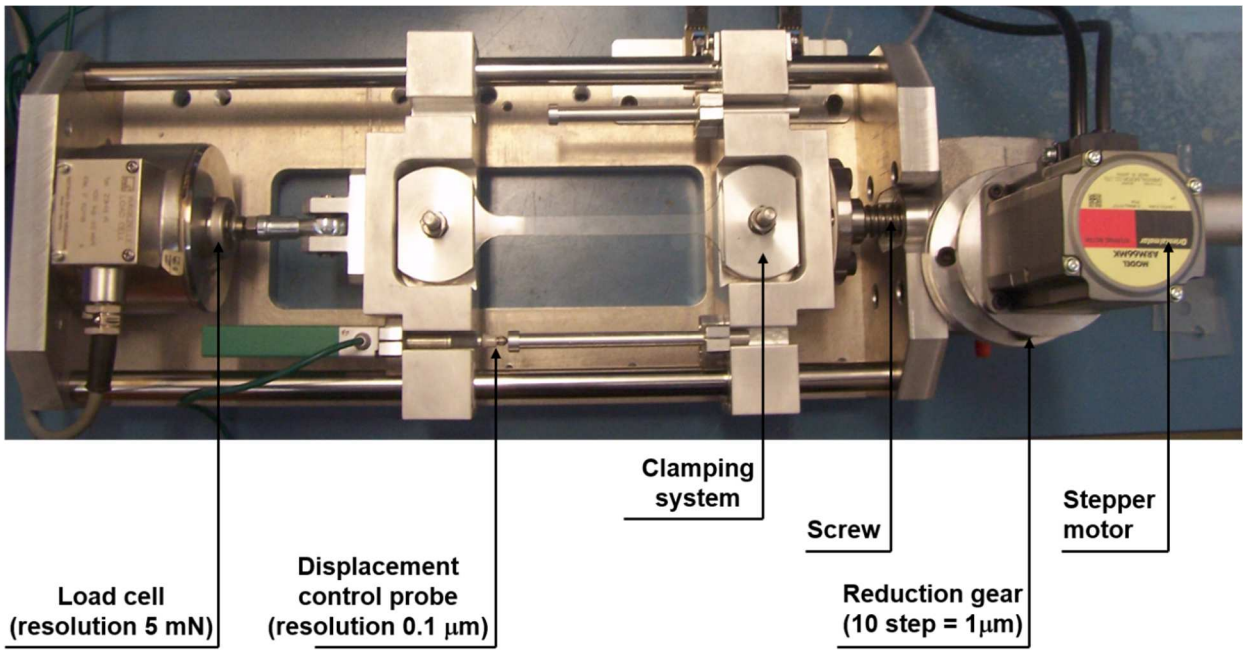

Figure 5 - Tensile elongation experimental setup.

Experimentally, Young’s modulus values are determined from the ratio between the incremental stress and the incremental strain applying the classical Hooke’s law at a constant strain rate,

$$E = \frac{\Delta\sigma}{\Delta\varepsilon} = \frac{F l_0}{A \Delta l} \qquad \textit{Equation 22}$$

where E is the Young's modulus (Pa), $\Delta\sigma$ is the incremental stress (Pa), $\Delta\varepsilon$ is the incremental strain (dimensionless), F is the tensile force (N), A is the surface area of the sample (m^2) on which the force acts, l_0 is the initial length of the sample (m), and Δl is the deformation (m) resulting from the application of F within the region in which the sample under investigation shows an elastic behaviour.

Table 1 – Overview of all measurements

Measurement type	**Length scale**	**Measurement scope**	**Loading rate / time**	**Holding force / strain**	**Holding time**	**Temperature (℃)**	**Humidity (%)**	**Estimated material property**
Berkovich Nanoindentation	Nano	Surface	1-3-10 s	0.2 mN	10 to 3000 s	23.6	40	E^*_0, E^*_∞
Flat punch Nanoindentation	Nano	Surface	5 s	0.2 mN	130 s	25	47	E^*_0, E^*_∞
Normal Relaxation	Meso	Bulk	0.013 mms^{-1}	5%-10%-15%	1800 s	24	-	E_0, E_∞
Normal Compression	Meso	Bulk	0.16 mms^{-1}	5%-10%-15%	12.4s (cycle)	24	-	E
Tensile test	Meso	Bulk	0.01 to 0.1 mms^{-1}	-	-	21	-	E
Shore A hardness	Meso	Surface	-	-	-	24	-	E

Chapter 3

EXPERIMENTAL RESULTS

3.1. Nanoindentation Creep

3.1.1. Berkovich Tip

As expected, the material did not reach an equilibrium state during the nanoindentation creep experiments. The material continues to deform in prolonged tests, as demonstrated in experiments run up to 3000 seconds (Figure 6). Hence, $E(\infty)$ (found using Equation 6) should be considered an extrapolation of the fit rather than a determined value.

We first curve-fitted the 5-parameter (2-arm) Kelvin Voigt model to the resulting creep curves (Figure 6). Next, we estimated the average values of the indentation moduli E_0* and E_∞* for different hold times (Figure 7). The indentation moduli were then converted to E_0 and E_∞ to facilitate comparison with other measurements. The modulus values showed no correlation with loading time but correlated negatively with holding time.

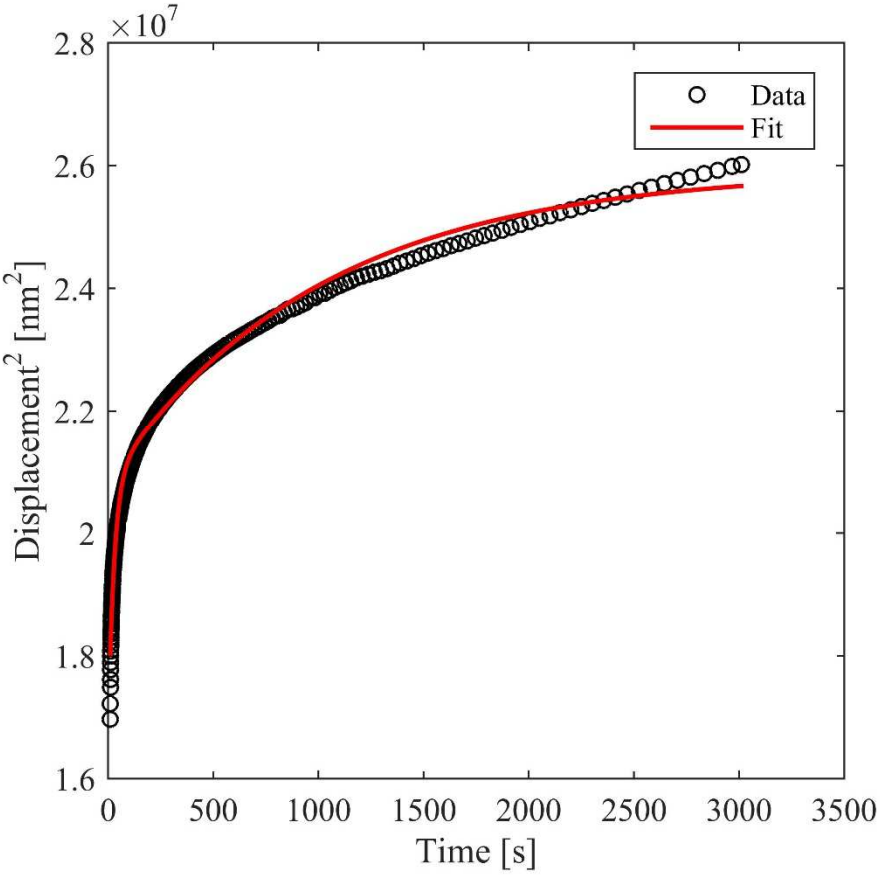

Figure 6 - Sample Berkovich indentation creep curve fit (t_{hold} = 3000s).

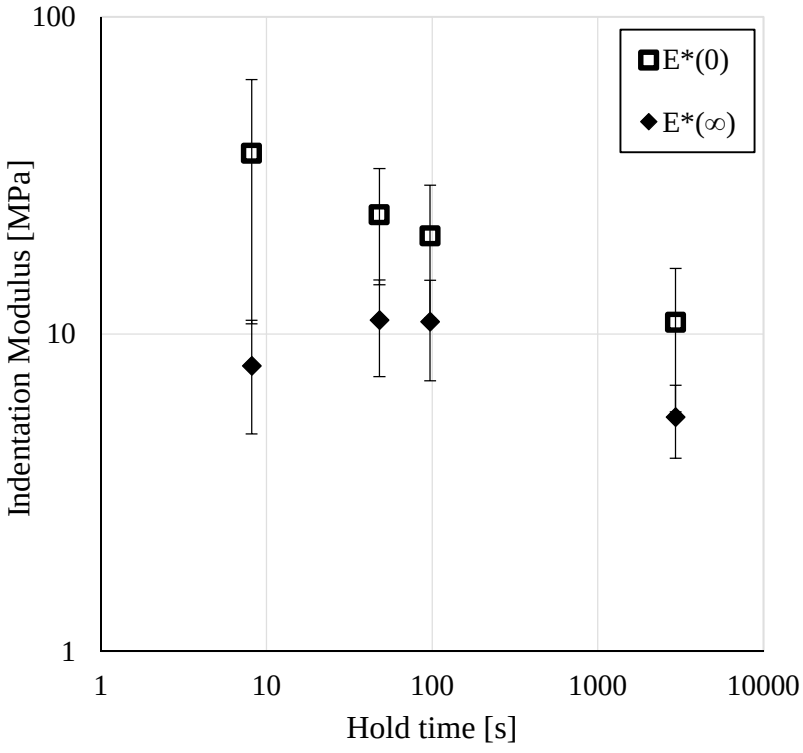

Figure 7 – The results of the creep experiments performed with the Berkovich indenter.

The mean indentation moduli (averaged over the hold times) were E^*_0 = 22.6 ± 17.4 MPa and E^*_∞ = 8.76 ± 3.86 MPa. Using these values in Equation 6 and Equation 7, we estimated the mean instantaneous and steady state elastic moduli as E_0 = 17.0 ± 13.0 MPa and E_∞ = 6.66 ± 2.90 MPa, respectively.

3.1.2. Flat Punch Tip

We estimated the indentation moduli as E^*_0 = 17.95 ± 3.52 MPa and E^*_∞ = 13.62 ± 2.00 MPa. The instantaneous and steady state elastic moduli were estimated as E_0 = 13.46 ± 2.639 MPa and E_∞ = 10.22 ± 1.50 MPa, respectively.

3.2. Mesoscale Measurements

3.2.1. Shore hardness

The polychloroprene rubber's Shore hardness (53A) was converted to elastic modulus using Equation 11. We estimated the elastic modulus as 5.64 MPa.

3.2.2. Normal compression

The resulting stress-strain curves show some hysteresis during compression (Figure 8), which is expected from a viscoelastic material. The preconditioning phase of the experiment shows a difference between the first and tenth loading-unloading cycles. However, after cycle 10 the cycles overlapped. The material is also evidently non-linear in compression. The material also showed insignificant variation of modulus value between different strain loading rates (Figure 9).

The ISO 7743:2008 standard suggests reporting the elastic modulus in the compression segment of the final cycle at 10% normal strain, which was calculated as 0.648 MPa (for the strain loading rate of 0.16 mms^{-1}. For comparison, the elastic moduli at 5% strain and 15% strain were also calculated from the stress-strain curve as 0.271 and 0.935 MPa, respectively.

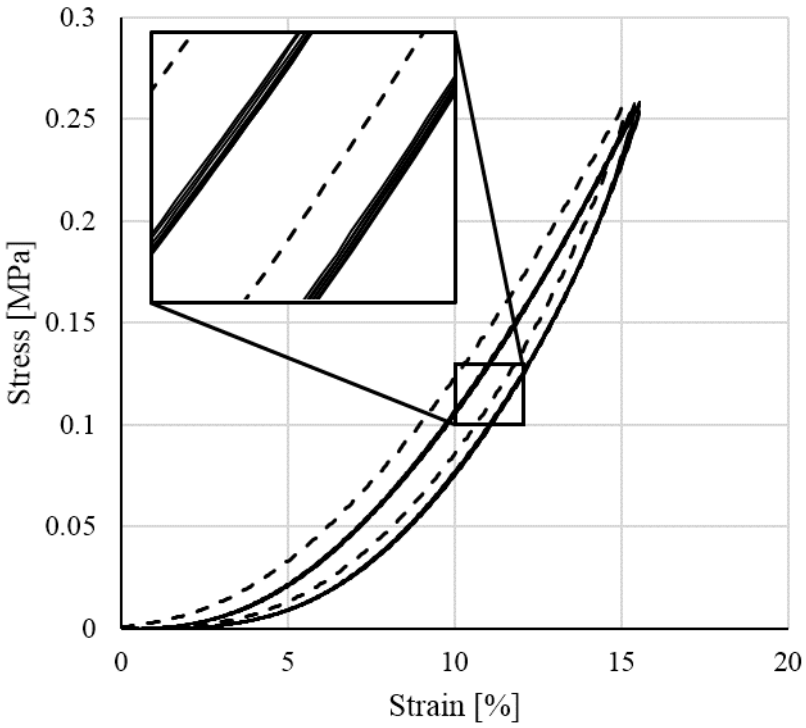

Figure 8 – Stress-strain curves for cycle 1 (dashed line) and cycles 10 - 17 (solid lines) of the Neoprene (boxed section magnified).

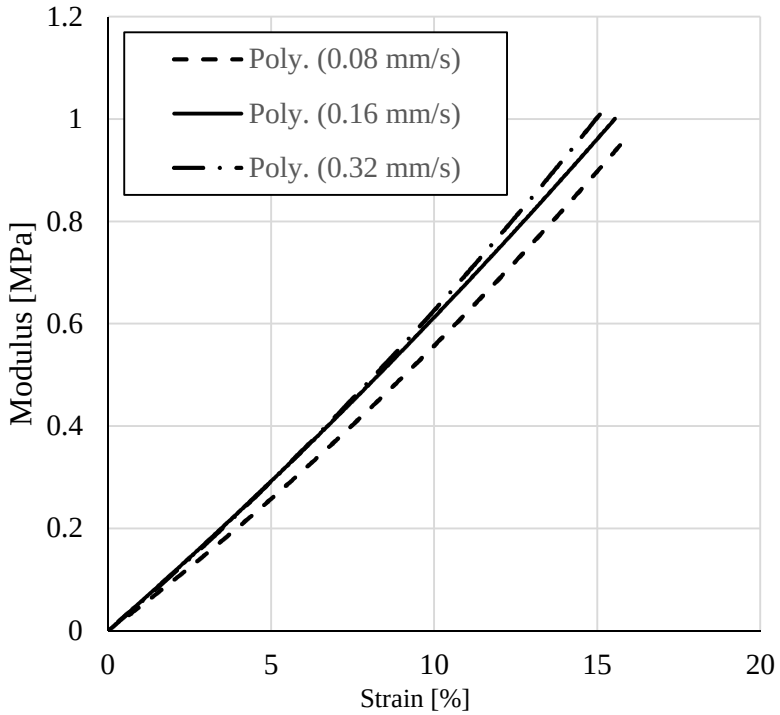

Figure 9 - Elastic modulus versus strain for loading rates of 0.08 mms^{-1} (dashed line), 0.16 mms^{-1} (solid line), and 0.32 mms^{-1} (dash-dotted line).

3.2.3. Normal relaxation

We curve-fitted different model sizes to the experimental results, finding the 2-arm (5-parameter) Maxwell model to be the most suitable (Figure 10). The 1-arm (i.e. 1-element) model did not provide a sufficiently accurate fit and the 3-arm model had non-singular coefficient results.

We estimated the relaxation modulus for 5%, 10%, and 15% normal strain by curve-fitting a 5-parameter Maxwell model to the relaxation curves (Figure 11). The instantaneous elastic modulus, $E_{0,}$ varied between 0.5 to 1.43 MPa and the steady state elastic modulus, E_{∞}, varied between 0.36 to 0.98 MPa for the normal strain varying from 5%-15%.

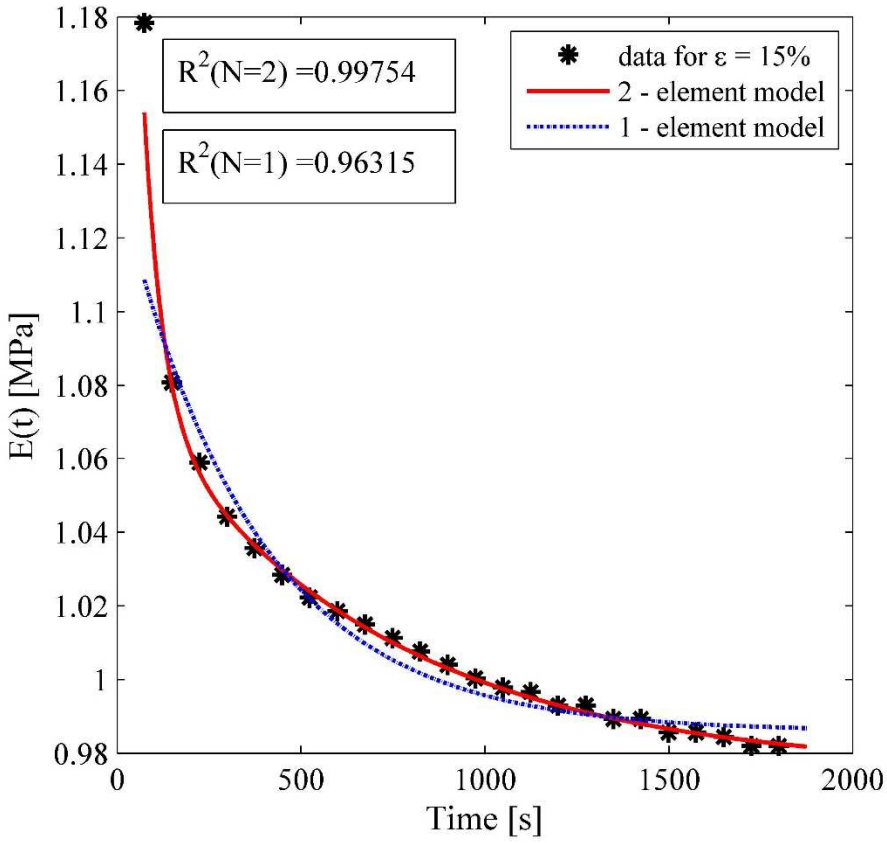

Figure 10- Comparison of different Maxwell model sizes in fitting relaxation data. Regression values are written above curves.

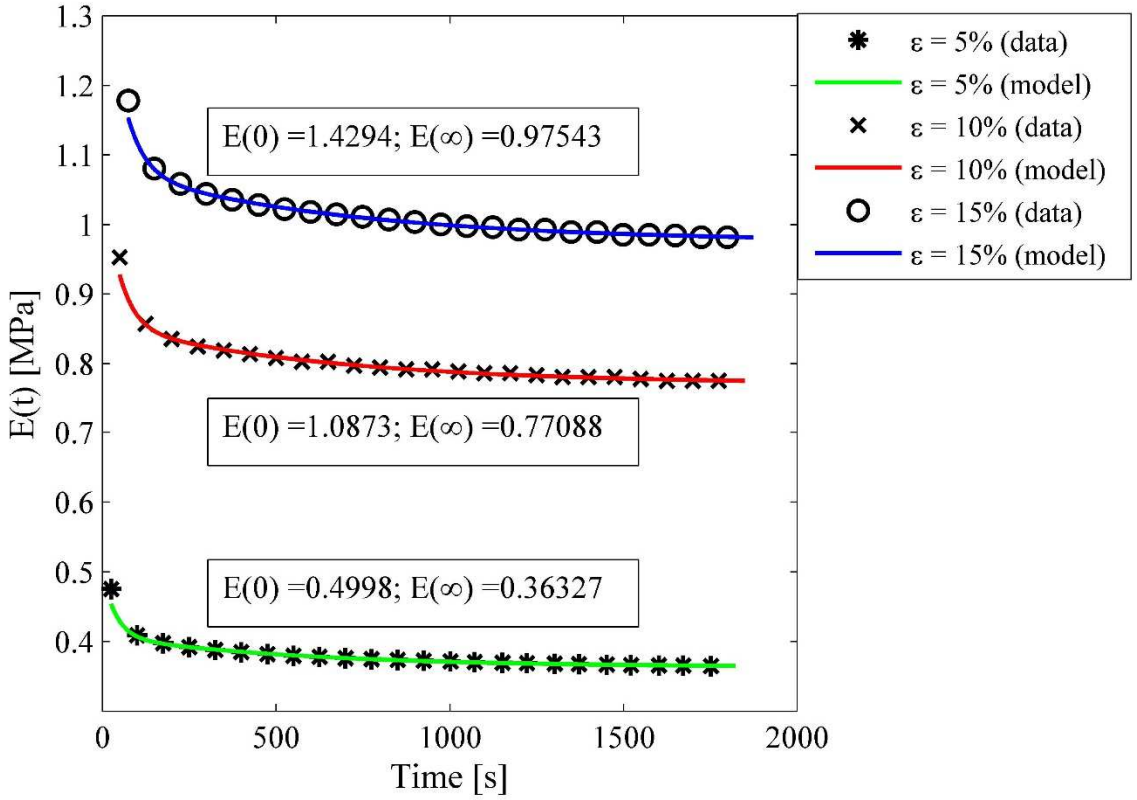

Figure 11 – The change in relaxation modulus as a function of time for normal strains of 5% (green), 10% (red), and 15% (blue).

3.2.4. Tensile Test

The effect of loading rate on Young's modulus is shown in Figure 12. Standard deviations were calculated based on an overall uncertainty accumulation of 7.3%. Using a second order polynomial curve fitting, the Young's modulus corresponding to zero strain rate was estimated as 1.24 ± 0.1 MPa.

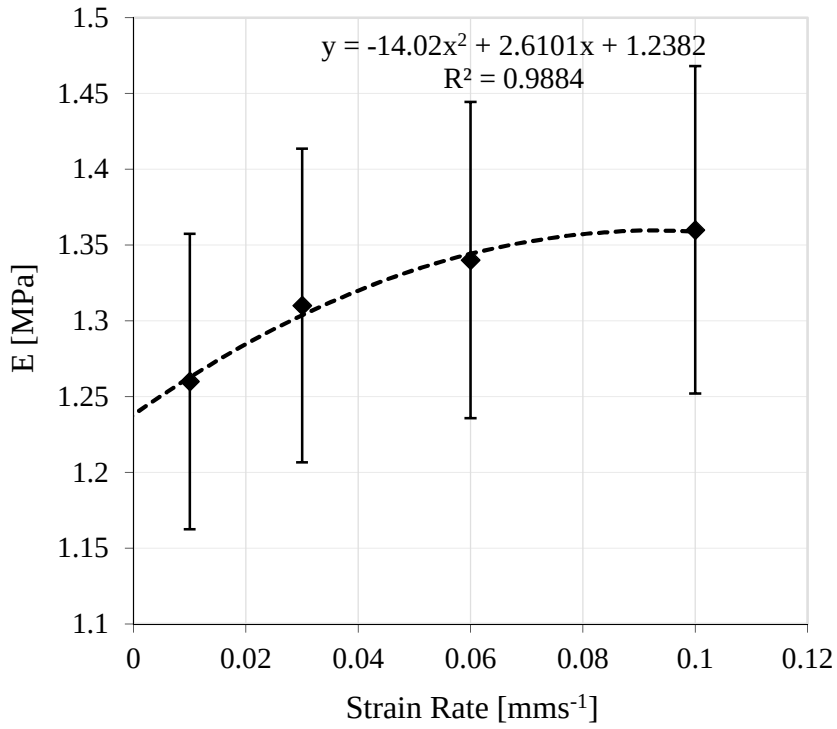

Figure 12 – Results of the tensile test.

Chapter 4

DISCUSSION

The goal of our research was to compare the material properties of neoprene rubber estimated by an array of characterization performed at nano and meso scales. To facilitate this goal, we conducted nanoindentation and conventional compression and tension experiments and selected material parameters that can be readily compared in a common framework (Table 1, Figure 13). We first discuss our results and then compare them with those of other earlier studies.

4.1. Discussion of current results

The tensile test provided us with a widely-accepted measure of tensile Young's modulus. The tensile test also showed that neoprene exhibits rate-dependent viscoelastic behavior, even at low loading velocities of 0.1 mms^{-1}. The Young modulus obtained by the tensile test (1.24 MPa) was comparable to those obtained by the compression experiments, but much lower than those obtained by the nanoindentation experiments.

However, deformations of an incompressible hyperelastic material during indentation mimic those of a normal compression test better than similar deformations in a tensile test. In more technical terms, deformation states of surface indentation measurements lie closer to those of uniaxial compression than to those of uniaxial tension measurements in the invariant planes (for more details, see [34] and [35]). Hence, we believe that the results of nanoindentation experiments are more credibly compared with normal compression experiments at the mesoscale. The steady state elastic modulus estimated by the quasi-static compression experiments was significantly lower than those of the nanoindentation experiments (E_∞ = 0.648

MPa via normal compression versus 6.57 MPa via Berkovich tip and 10.22 MPa via flat-punch tip indenters). The relaxation experiments performed in the normal direction also returned lower instantaneous and steady state moduli than those of the creep experiments performed at the nanoscale (Figure 13).

There could be several reasons for this discrepancy between the results of experiments performed at nano and meso scales. Firstly, it can be an artifact of the experimental scale; the smaller scale may cause different stiffness mechanisms to react to the experimental input. Secondly, the surface material properties of the Neoprene rubber could be simply higher than its bulk properties. During the manufacturing of the rubber sheets, rolling and surface finishing processes are applied which may lead to a stiffer surface. In fact, the modulus value estimated by our Shore-A hardness measurements, which is a mesoscale measurement of the surface response, was indeed higher than those of the tension and compression experiments (5.64 MPa versus 1.24 and 0.648 MPa, respectively; Figure 13).

Previously, Champhekar [11] conducted quasistatic nanoindentation with a blunt tip and found a negative correlation between the indentation depth and the measured modulus values for various viscoelastic materials. He attributes this observation to instrumental and analytical errors and higher material stiffness on the surface and lower stiffness in the bulk. Lim and Chaudhri [12] also performed nanoindentation on variety of polymers using a Vickers tip and observed similar trends. They suggested frictional effects for the observed discrepancies, which were later confirmed by finite element analysis by Kamran and Larsson [36].

Alternatively, modeling assumptions proven correct in the mesoscale may no longer be applicable in smaller scales (more details in [11] and [14]). For example, in flat-punch indentation nonlinearities may cause an overestimation of the modulus value. Larsson and Carlsson [37] suggest that linearity is only valid for ratios of indentation depth to contact area

radius (h/R) lower than 0.05. This ratio for our flat-punch reached 0.54, which resulted in modulus values in the order of 10 MPa. Additionally, stress concentrations caused by the sharp tip of the Berkovich indenter may also artificially increase estimated modulus values.

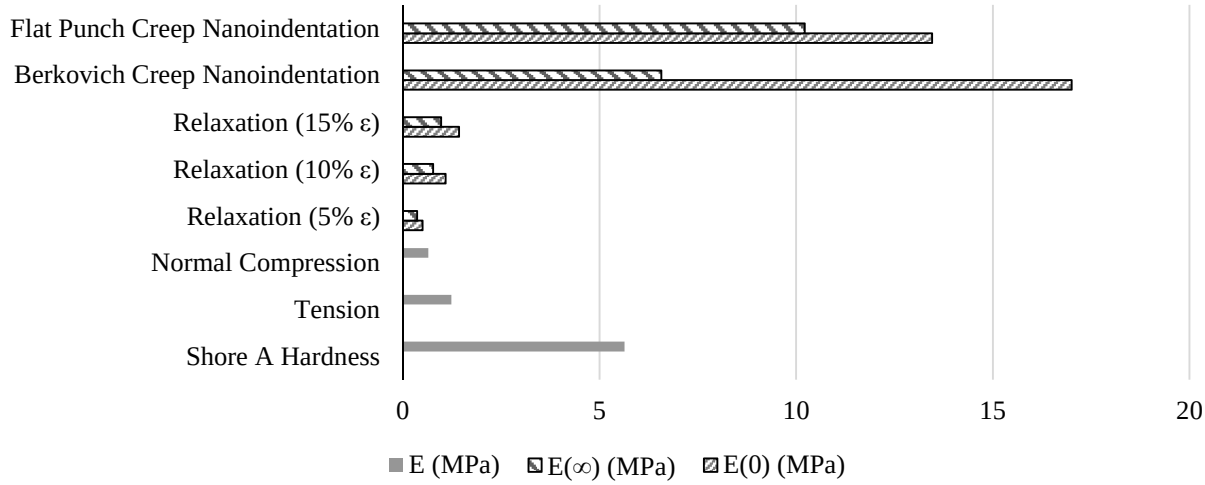

Figure 13 – Summary of results of all experiments performed at nano and meso scales.

4.1.1. Departure from continuum mechanics

In this research, we assumed the material follows continuum laws in deformation, both in the mesoscale and the nanoscale. Continuum mechanics ignores the structure of a material on the molecular scale, taking that the volume is continuously distributed and can be divided indefinitely. In view of this assumption, an infinitesimal particle can be defined, inside of which strain tensors form in response to stress tensors caused by force loading. When an elastic material is deformed by a unidirectional force, this particle obtains the energy potential [38]

$$W = \frac{1}{2}\lambda\varepsilon_{ii}\varepsilon_{jj} + \mu\varepsilon_{ji}\varepsilon_{ij}, \qquad \textit{Equation 23}$$

where λ and μ are Lame's constants, ε_{ij} is the infinitesimal strain tensor, and W is the total deformation energy density. However, as detailed by Nikolov et al. [38], there may be additional energy potentials in the material that are not accounted for in a continuum mechanics analysis. These contributions follow from the mechanics of the material's molecular structure.

If these contributions are significant, Nikolov shows that the deformation energy density would instead follow

$$W = \frac{1}{2}\lambda\varepsilon_{ii}\varepsilon_{jj} + \mu\varepsilon_{ij}\varepsilon_{ji} + \frac{\widetilde{K}}{3}\chi^{s}_{ij}\chi^{s}_{ij} \qquad \textit{Equation 24}$$

where the final term accounts for Frank elasticity energy, expressed through the effective Frank constant $\widetilde{K}$(Newtons) and the symmetric curvature tensor χ^{s}_{ij}. This additional term is found by assuming additional rotational gradients due to molecular dynamics effects in the material, which includes energy potentials added through molecular chain interactions. These contributions are considered to be negligible in continuum mechanics but may be significant here due to the smaller length scale in the nanoindentation experiments.

Following the couple stress theory approach developed by Yang et al. [39], a characteristic length *l* is introduced to describe the extent of local effects. This length scale has been previously found to be ~0.25 nm for most metals, ~0.82 nm for gallium arsenide, and ~3.3 nm for graphite. Using the Frank energy constant for main chain polymers, Nikolov et al. found the length scale for main-chain polymers to be ~4.6 nm. This implies that in the case of rubber polymers, size effects due to significant strain gradient contributions happen in the size domain of a few nanometers. This hypothesis is later verified by Han [40] using data from common main-chain polymers (e.g. UHMWPE, PTFE/Teflon), which show no size effects in the length scales measurable with nano- and microindentation. Likewise, our material polycholoroprene (Neoprene) consists of chloroprene molecules knit together in chains, so it is expected that such size effects will be similarly absent. Thus, a departure from continuum mechanics and a requirement to consider molecular mechanics in the material response is not needed when our measurement length scales are far from 4.6 nanometers. In view of this conclusion, we believe that the continuum mechanics assumption holds valid for our nanoindentation experiments in addition to the mesoscale measurements.

We must note however that size effects due to Frank energy potential were previously found to partially explain size effects in the nanoindentation of polydimethylsiloxane (PDMS) [14]. Wrucke et al. [14] had conducted quasistatic nanoindentation experiments on PDMS with a Berkovich tip at test depths from 200 nm to 100 µm. They observed that the hardness value, which is assumed to be linearly proportional to the material's elastic modulus, increased by several orders of magnitude with decreasing indentation depth. They attributed this observation to molecular interactions based on Frank Energy and also a possibly harder material surface.

4.1.2. Data scatter in nanoindentation

There appears to be a higher scatter of data (i.e. higher standard deviation) for nanoindentation results. Further investigation of the samples using scanning electron and optical microscopy (Figure 14) revealed material inhomogeneity (which may be attributed to the rubber's filler content) and cracks on the surface. The cracks ranged in width from a few nanometers up to 1 µm. These two phenomena may be the cause of the large results deviations that we have observed in the nanoscale measurements. The indentation contact areas were in the few micrometers (4.75 µm for flat-punch, and up to 22 µm for the Berkovich tip), similar in size to some observed inhomogeneities. Champhekar [11] had also observed this in his Neoprene samples. There was also higher standard deviations at lower hold times in the Berkovich indentation. This is expected, as with lower hold times the material has less time to creep and becomes more sensitive to local surface and loading conditions. Also, as the indenter controller began force loading, certain variations aggravated by the softness of the Neoprene sample caused the loading to deviate from ideal constant-rate conditions. Measurements at lower hold times are more affected by these deviations. In addition, a lower hold time provides less data for curve fitting, making the fit more variable.

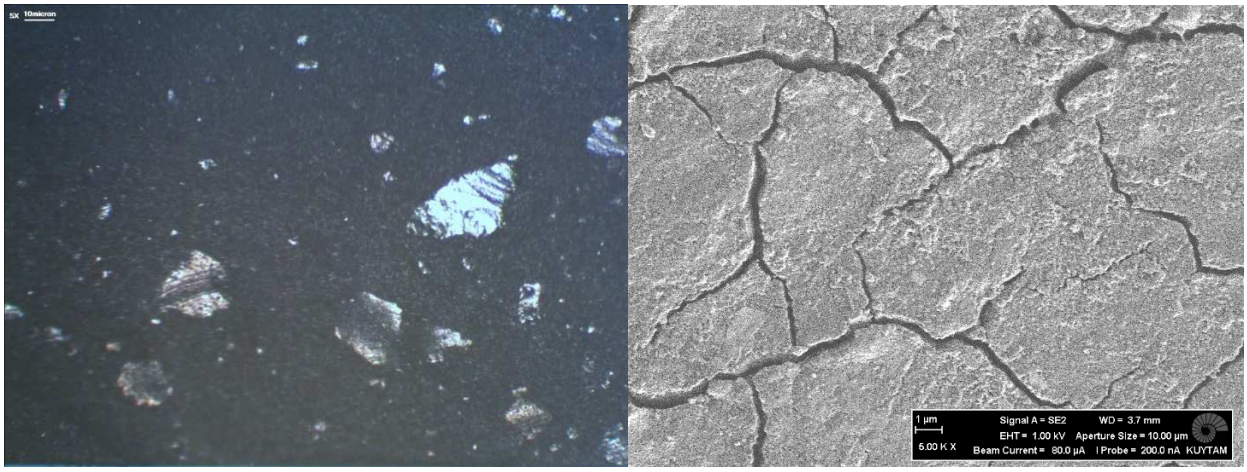

Figure 14 – Optical microscope (left, 5x) and scanning electron microscope (right, 5000x) images of one polychloroprene (Neoprene) sample.

4.2. Comparison of nanoindentation results with those of earlier indentation studies

The results of our nanoindentation experiments show a good agreement with those of earlier studies. Champhekar [11] performed quasi-static indentations on Neoprene rubber using a blunt conico-spherical indenter having a tip diameter of 5 µm and an included angle of 60^0. The experiments were conducted in the depth rage of 0.1 to 2.5 µm, such that only the spherical tip was in contact with the material. They observed that modulus values are depth-dependent, with higher moduli at lower depths (varied between 50 and 9 MPa, Figure 15). On the basis that a similar trend was also observed for three other viscoelastic materials, they concluded that this increase was a modeling artifact. Their model assumed contact area is the same as in conico-pyramidal indentation, whereas it differs. Lim and Chaudhri [26] also estimated the elastic modulus values of Neoprene rubber via nanoindentation. They initially used a tungsten carbide ball of 4 mm in diameter to perform quasi-static indentation experiments and estimated the elastic modulus as 8.15 MPa (depth of indentation was ~180 µm). Their second experiment performed with a Vickers indenter tip returned modulus values of 21 and 9 MPa for the indentation depths of 9 and 100 µm, respectively [12]. Similar to Champhekar's [11] results, their modulus values also decreased logarithmically as the indentation depth was increased (Figure 15). Among their explanations, Kamran and Larsson [36] later confirmed through finite

element analysis that frictional effects on the Vickers indenter's ridges are responsible for their observed discrepancies.

We must note that most previous research on polychloroprene considered only the elastic response and ignored the viscous component. However, as apparent in our results, the viscous component contributes greatly to the overall mechanical response. Champhekar [11] conducted nanoDMA measurements on neoprene rubber, but their frequency domain response cannot be aptly compared with our time domain results. The previous measurements also used different indenter tips and measurement protocols. In addition, material chemical composition may be another source of discrepancy. Hence, our comparisons with earlier measurements are tentative.

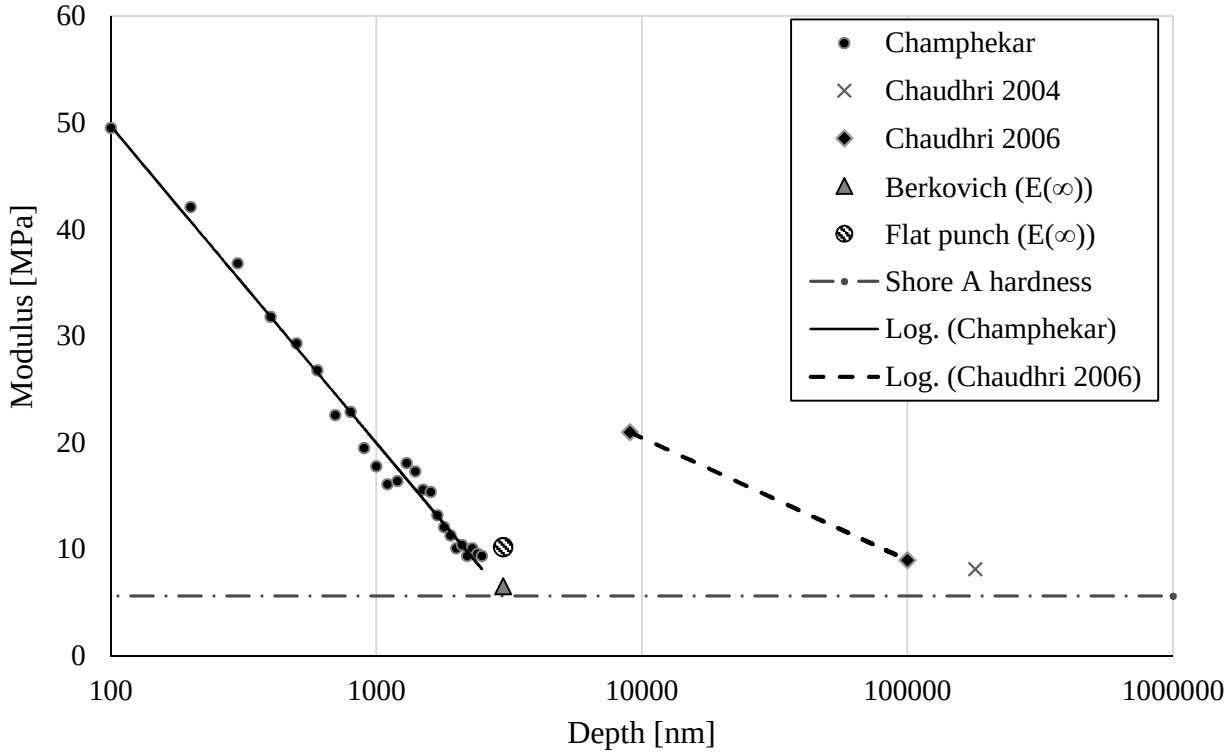

Figure 15 – Comparison of modulus values reported for Neoprene rubber in our nanoindentation experiments with those of earlier studies.

Chapter 5

CONCLUSIONS

We conducted a research study to evaluate the material properties of polychloroprene (Neoprene) rubber with an array of characterization experiments performed at the nano and meso scales. These experiments were performed by 4 different research groups independently on the same rubber samples. We first compared our results between the groups and afterwards with those of other earlier studies. Since the experiments were performed by different devices under different experimental conditions and protocols, we selected the most fundamental material property, elastic modulus, as the medium of comparison. We also utilized equivalent viscoelastic models for compatibility (i.e. 2-arm Generalized Maxwell and Kelvin-Voigt models for relaxation and creep responses of the material). The model parameters were estimated by curve-fitting the experimental data. The results of our experiments showed that nanoindentation experiments returned higher modulus values and scatter in the experimental data than those obtained by the mesoscale experiments. In addition, our nanoindentation results show good agreement with previous indentation experiments on Neoprene rubber.

BIBLIOGRAPHY

[1] D. Ebenstein, L. Pruitt, Nanoindentation of biological materials, Nano Today. 1 (2006) 26–33. http://www.sciencedirect.com/science/article/pii/S1748013206700779 (accessed December 22, 2014).

[2] D.C. Lin, F. Horkay, Nanomechanics of polymer gels and biological tissues: A critical review of analytical approaches in the Hertzian regime and beyond, Soft Matter. 4 (2008) 669. doi:10.1039/b714637j.

[3] M.L. Oyen, Nanoindentation of Biological and Biomimetic Materials, Exp. Tech. 37 (2013) 73–87. doi:10.1111/j.1747-1567.2011.00716.x.

[4] V.T. Nayar, J.D. Weiland, A.M. Hodge, Macrocompression and Nanoindentation of Soft Viscoelastic Biological Materials, Tissue Eng. Part C Methods. 18 (2012) 120719071355005. doi:10.1089/ten.tec.2012.0034.

[5] R.F. Gibson, A review of recent research on nanoindentation of polymer composites and their constituents, Compos. Sci. Technol. 105 (2014) 51–65. doi:10.1016/j.compscitech.2014.09.016.

[6] A.M. Díez-Pascual, M. a. Gómez-Fatou, F. Ania, A. Flores, Nanoindentation in polymer nanocomposites, Prog. Mater. Sci. 67 (2015) 1–94. doi:10.1016/j.pmatsci.2014.06.002.

[7] N. Moharrami, S.J. Bull, A comparison of nanoindentation pile-up in bulk materials and thin films, Thin Solid Films. 572 (2014) 189–199. doi:10.1016/j.tsf.2014.06.060.

[8] J.M. Antunes, J. V. Fernandes, N.A. Sakharova, Anti-Abrasive Nanocoatings, Elsevier, 2015. doi:10.1016/B978-0-85709-211-3.00016-9.

[9] D. a. Lucca, K. Herrmann, M.J. Klopfstein, Nanoindentation: Measuring methods and applications, CIRP Ann. - Manuf. Technol. 59 (2010) 803–819. doi:10.1016/j.cirp.2010.05.009.

[10] M. VanLandingham, Nanoindentation of polymers: an overview, Macromol. Symp. 167 (2001) 15–44. http://www.sciencedirect.com/science/article/pii/S0040609014008189 (accessed January 6, 2015).

[11] M.C. Champhekar, Viscoelastic Properties of Polymers: A Comparison of Micro and Macro Scales at North Carolina State University, (2013).

[12] Y.Y. Lim, M.M. Chaudhri, Indentation of elastic solids with a rigid Vickers pyramidal indenter, Mech. Mater. 38 (2006) 1213–1228. doi:10.1016/j.mechmat.2006.04.006.

[13] E.G. Herbert, W.C. Oliver, A. Lumsdaine, G.M. Pharr, Measuring the constitutive behavior of viscoelastic solids in the time and frequency domain using flat punch nanoindentation, J. Mater. Res. 24 (2009) 626–637. doi:10.1557/jmr.2009.0089.

[14] A.J. Wrucke, C.-S. Han, P. Majumdar, Indentation size effect of multiple orders of magnitude in polydimethylsiloxane, J. Appl. Polym. Sci. 128 (2013) 258–264. doi:10.1002/app.38161.

[15] H. Hertz, Ueber die Berührung fester elastischer Körper., J. Für Die Reine Und Angew. Math. (Crelle's Journal). (1882) 146–162. doi:10.1515/crll.1882.92.156.

[16] I. Sneddon, The relation between load and penetration in the axisymmetric Boussinesq problem for a punch of arbitrary profile, Int. J. Eng. Sci. 3 (1965) 47–57. http://www.sciencedirect.com/science/article/pii/0020722565900194 (accessed January 20, 2015).

[17] W. Oliver, G. Pharr, An improved technique for determining hardness and elastic modulus using load and displacement sensing indentation experiments, J. Mater. Res. 7 (1992) 1564–1583. http://journals.cambridge.org/abstract_S0884291400017039 (accessed December 22, 2014).

[18] P.-E. Mazeran, M. Beyaoui, M. Bigerelle, M. Guigon, Determination of mechanical properties by nanoindentation in the case of viscous materials, Int. J. Mater. Res. 103 (2012) 715–722. doi:10.3139/146.110687.

[19] M. a. Monclus, N.M. Jennett, In search of validated measurements of the properties of viscoelastic materials by indentation with sharp indenters, Philos. Mag. 91 (2011) 1308–1328. doi:10.1080/14786435.2010.504197.

[20] J. Kaufman, G. Miller, Time-dependent mechanical characterization of poly (2-hydroxyethyl methacrylate) hydrogels using nanoindentation and unconfined compression, J. Mater. Res. 23 (2008) 1472–1481. doi:10.1557/JMR.2008.0185.Time-dependent.

[21] F. Carrillo, S. Gupta, M. Balooch, S.J. Marshall, G.W. Marshall, L. Pruitt, et al., Nanoindentation of polydimethylsiloxane elastomers: Effect of crosslinking, work of adhesion, and fluid environment on elastic modulus, J. Mater. Res. 20 (2005) 2820–2830. doi:10.1557/JMR.2005.0354.

[22] K.L. Johnson, Contact Mechanics, Cambridge University Press, Cambridge, U.K., 1987.

[23] L. Cheng, X. Xia, W. Yu, Flat-punch indentation of viscoelastic material, J. Polym. …. 38 (2000) 10–22. http://onlinelibrary.wiley.com/doi/10.1002/(SICI)1099-0488(20000101)38:1%3C10::AID-POLB2%3E3.0.CO;2-6/full (accessed January 5, 2015).

[24] Z. Wang, A. a. Volinsky, N.D. Gallant, Nanoindentation study of polydimethylsiloxane elastic modulus using Berkovich and flat punch tips, J. Appl. Polym. Sci. 132 (2015) n/a–n/a. doi:10.1002/app.41384.

[25] J. Kunz, M. Studer, Determining the Modulus of Elasticity in Compression via the Shore A Hardness, Kunststoffe Int. 6 (2006) 1–3. https://www.kunststoffe.de/en/journal/archive/article/component-design-determining-the-modulus-of-elasticity-in-compression-via-the-shore-a-hardness-588533.html (accessed December 18, 2014).

[26] Y.Y. Lim, M.M. Chaudhri, Indentation of elastic solids with rigid cones, Philos. Mag. 84 (2004) 2877–2903. doi:10.1080/14786430410001716782.

[27] E.S. Berkovich, Three-Faceted Diamond Pyramid for Studying Microhardness by Indentation, Zavod. Lab. 13 (1950) 345–347. papers2://publication/uuid/2ABF5102-54AB-4352-A596-329F788A2EA2.

[28] E.H. Lee, J.R.M. Radok, The Contact Problem for Viscoelastic Bodies, J. Appl. Mech. 27 (1960) 438. doi:10.1115/1.3644020.

[29] M.L. Oyen, Analytical techniques for indentation of viscoelastic materials, Philos. Mag. 86 (2006) 5625–5641. doi:10.1080/14786430600740666.

[30] J. Ferry, Viscoelastic Properties of Polymers, Wiley, New York City, U.S., 1970.

[31] P.B. Lindley, Engineering Design With Natural Rubber., Malaysian Rubber Producers' Research Association, Kuala Lumpur, Malaysia, 1974.

[32] a. R. Freakley, P. K., and Payne, Theory and Practice of Engineering with Rubber, Elsevier Applied Science Publishers, Limited, 1978. http://books.google.com.tr/books?id=3Id5QgAACAAJ.

[33] M. Sedef, Particle-based modeling of non-linear viscoelastic deformable objects based on experimental data, (2008).

[34] Z. Chen, T. Scheffer, H. Seibert, S. Diebels, Macroindentation of a soft polymer: Identification of hyperelasticity and validation by uni/biaxial tensile tests, Mech. Mater. 64 (2013) 111–127. doi:10.1016/j.mechmat.2013.05.003.

[35] M. Johlitz, S. Diebels, Characterisation of a polymer using biaxial tension tests. Part I: Hyperelasticity, Arch. Appl. Mech. 81 (2011) 1333–1349. doi:10.1007/s00419-010-0480-1.

[36] Y. Kamran, P.-L. Larsson, Second-order effects at microindentation of elastic polymers using sharp indenters, Mater. Des. 32 (2011) 3645–3653. doi:10.1016/j.matdes.2011.01.043.

[37] P.-L. Larsson, S. Carlsson, On microindentation of viscoelastic polymers, Polym. Test. 17 (1998) 49–75. doi:10.1016/S0142-9418(97)00038-X.

[38] S. Nikolov, C.S. Han, D. Raabe, On the origin of size effects in small-strain elasticity of solid polymers, Int. J. Solids Struct. 44 (2007) 1582–1592. doi:10.1016/j.ijsolstr.2006.06.039.

[39] F. Yang, a. C.M. Chong, D.C.C. Lam, P. Tong, Couple stress based strain gradient theory for elasticity, Int. J. Solids Struct. 39 (2002) 2731–2743. doi:10.1016/S0020-7683(02)00152-X.

[40] C.S. Han, Influence of the molecular structure on indentation size effect in polymers, Mater. Sci. Eng. A. 527 (2010) 619–624. doi:10.1016/j.msea.2009.08.033.

APPENDIX A

Parametric Study of Relaxation Model

We conducted a parametric study on the Generalized Maxwell model, which was used to fit the relaxation data. Our aim was to understand how each parameter in the normal relaxatıon curve-fitting formula influences the fit. As previously mentioned in Section 2.2.3, the curve-fitting formula is

$$E_{rel}(t) = E_{\infty} - \frac{E_1\tau_1}{t_0}\left(1 - e^{\frac{t_0}{\tau_1}}\right)e^{\frac{-t}{\tau_1}} - \frac{E_2\tau_2}{t_0}\left(1 - e^{\frac{t_0}{\tau_2}}\right)e^{\frac{-t}{\tau_2}} \qquad \textit{Equation A-1}$$

where E_{rel} is the relaxation modulus as a function of time (MPa), E_{∞} is the steady state response of the material (MPa), E_1 and E_2 are the spring constants of the two Maxwell arms (MPa), and τ_1 and τ_2 are the time constants of the two Maxwell arms (seconds). These model constants, in addition with t_0, the loading time (seconds), and t, time (seconds), define the material response. The loading time is constant for each experiment and E_{rel} is a function of t, so the varying coefficients left for curve-fitting are E_1, E_2, E_{∞}, τ_1, and τ_2.

The relaxation modulus function is a summation of 2 Maxwell arms and a steady-state response constant; we can understand the parameter effects by analyzing one isolated arm's response and considering how a summation of 2 such arms and a constant would fit the data. Each arm's relaxation response function is

$$E_{rel,arm}(t) = \frac{E\tau}{t_0}\left(e^{\frac{t_0}{\tau}} - 1\right)e^{\frac{-t}{\tau}} \qquad \textit{Equation A-2}$$

where E and τ are the arm's parameters (spring modulus and time constant, respectively). By varying these two constants over time, we find how each parameter affects the model response.

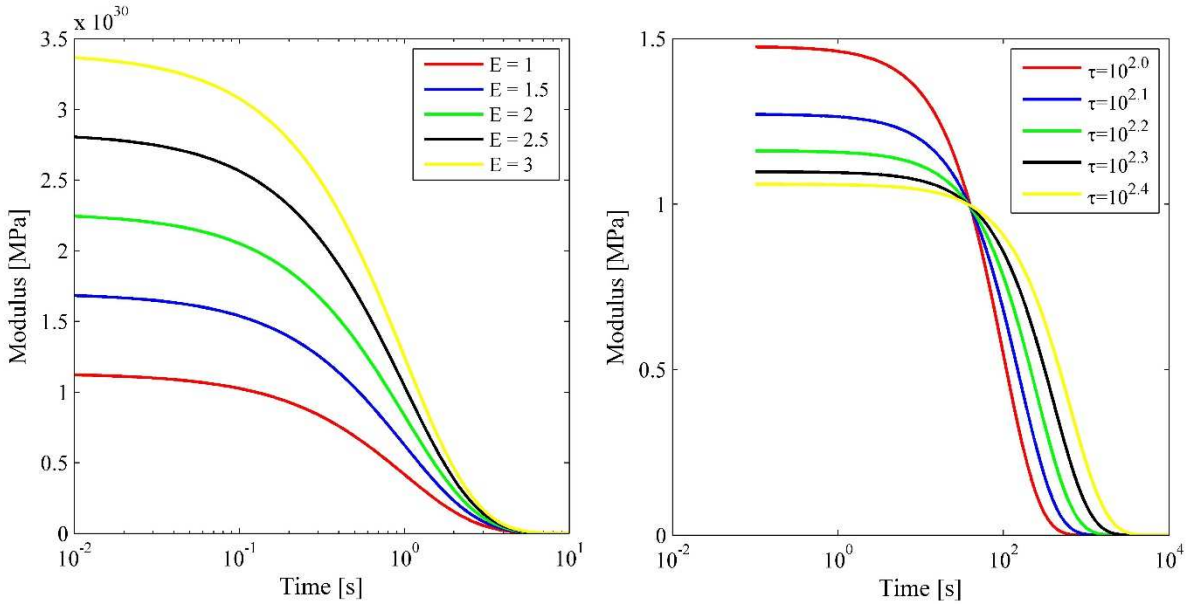

Figure 16- Modulus versus time for one Maxwell arm under ramp-and-hold loading. Varying E shows a scaling of the curve (left), while increasing τ pushes the curve rightward (right).

It is deducible that increasing each parameter affects the output curve differently (Figure 16). By increasing τ the plot shifts rightward, i.e. the material takes longer to relax. Increasing E increases the drop in relaxation modulus over time, i.e. the material has a higher instantaneous response. It also evident that the relaxation curve output has a linear relationship with E.

By combining two arms and the steady-state constant, we can understand how each parameter affects the fit. Each arm is distinguished based on its time constant (i.e. $\tau_i \neq \tau_j$). In our study, we chose τ_i indices with a higher j to represent larger time constants (i.e. $\tau_1 < \tau_2$). If after curve-fitting, two arms are found to have the same time constant ($\tau_i = \tau_j$) they must be considered as the same arm with an arm spring constant equal to the summation of the two arms ($E_k = E_i + E_j$). Hence, during curve-fitting, if two or more equal time constants are found for differing arms, the model size is downscaled to accommodate all equal-time-constant arms into one arm.

Figure 17, Figure 18, and Figure 19 show how each model parameter affects the fitted curve. The model parameters are varied in percentiles of their optimal fit value. Varying the time constants, τ_1 and τ_2, causes the curve to shift upward and rightward. The effect is more

pronounced in the lower time domain for the smaller time constant (τ_1) and more pronounced in the higher time domain for the larger time constant (τ_2). This is expected, as the $e^{-t/\tau}$ term, which explains each arm's dependence on time, shows dependency on τ. Changing each arm's spring coefficient, E_i, scales the response of the data upwards in the time domain where the arm has a more pronounced effect. In our case, the first arm affects mostly the beginning of the response, and likewise changing E_1 only alters the initial portion of the relaxation response curve. However, as the second arm has a higher time constant which causes it to affect larger time domains in the curve, E_2 alters a larger segment of the curve. Regarding the final variable, the steady-state response (E_∞), the change linearly translates the curve upwards.

We can see that each variable affects the curve to a different degree. Between the two arms, changing the coefficients of the arm with the higher time constant has a more prominent effect on the final fit. The steady state response, E_∞, appears to have the biggest effect, as it shifts the entire response in the vertical direction. The arm with the smaller time constant seems to have the smallest effect, changing the fit only in the initial portions of the relaxation response.

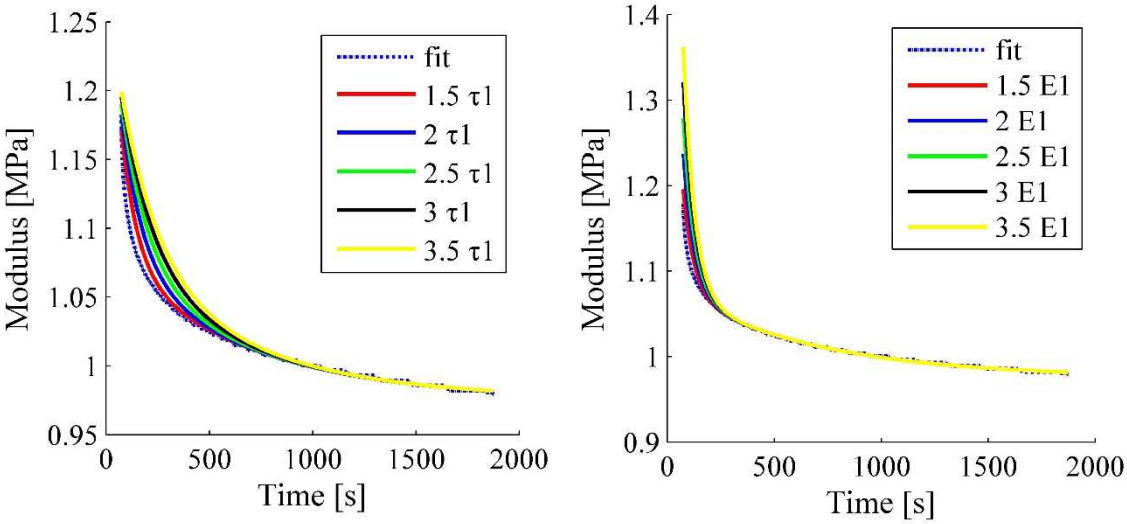

Figure 17 - Modulus versus time for model fit and parameter variations on first Maxwell arm (smaller τ).

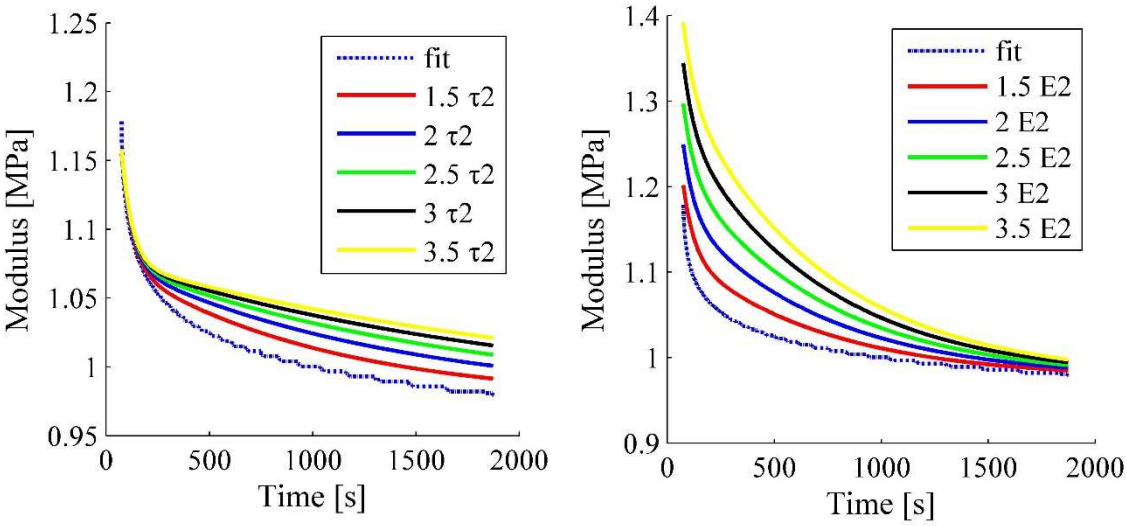

Figure 18 - Modulus versus time for model fit and parameter variations on second Maxwell arm (larger τ).

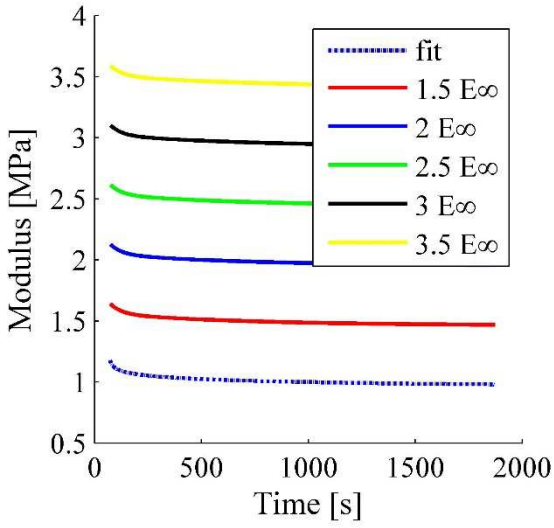

Figure 19 - Modulus versus time for model fit and parameter variations on steady-state response coefficient.

To quantitatively analyze the validity of these deductions, we drew a plot of R-squared (R^2) values versus percentage deviations of the different constants (E_∞, E_1, τ_1, E_2, τ_2) compared to their fitted value (Figure 20). In this plot, R^2 values are calculated as the regression-squared value between the fitted model and the experimental results. The R^2 value versus deviation of each parameter gives an approximation of how one coefficient affects the fit while other

coefficients are frozen. We can readily see that E_∞ shows the strongest change in R^2 when it deviates from its fitted value, as expected from Figure 19. Also as expected, E_1 and τ_1 marginally change R^2, whereas changes in E_2 and τ_2 prominently affect R^2.

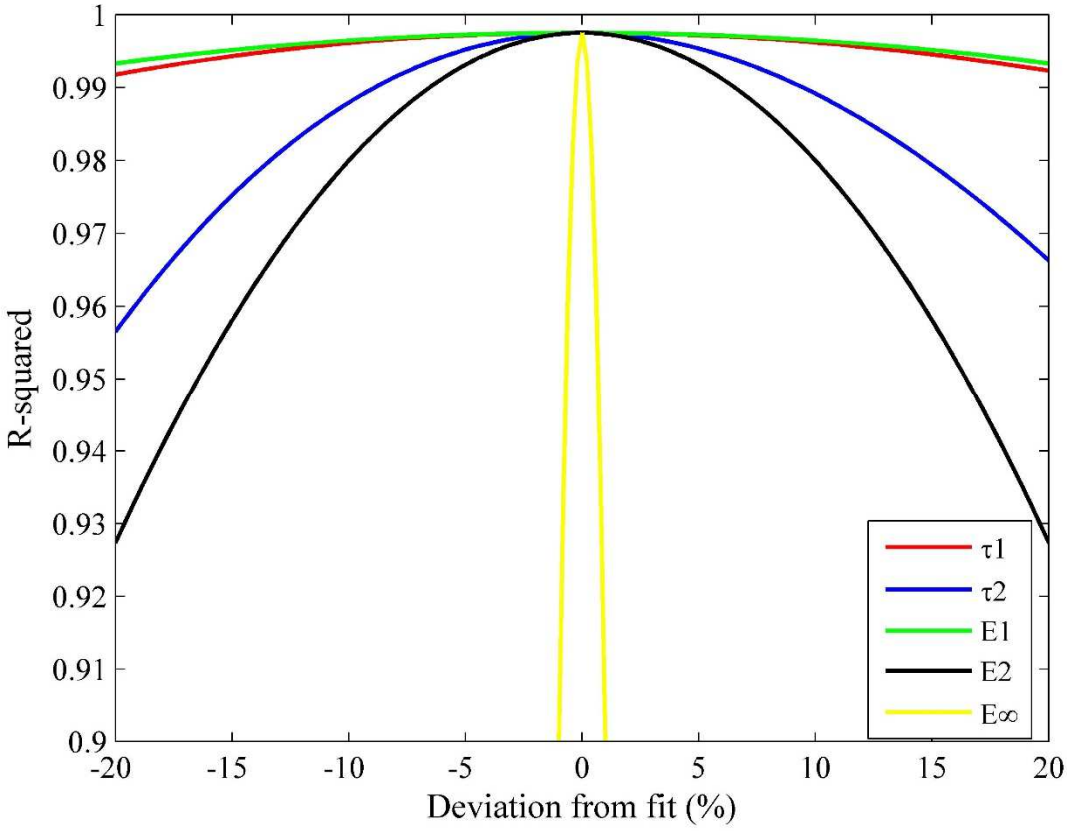

Figure 20 - R^2 value versus deviation for each model coefficient (with other coefficients held constant). The deviation percentage shows variations in each coefficient.

In conclusion, in our relaxation response model, the arm with the higher time constant has a larger effect on the measurement. This conclusion can be extended to Generalized Maxwell models with more than two arms. The effect of the arm with the lower time constant is more prominent in the lower part of the time domain. Changing the elastic spring coefficient of each arm, E, scales the relaxation response of that arm in the vertical direction (i.e. relaxation modulus axis). However, changing the time constant, τ, affects both the absolute value of the relaxation response and also how it dissipates over time (i.e. the curve is scaled in both vertical and horizontal directions). The steady-state response spring constant, E_∞, shifts the model's

plot in the vertical direction. R^2 analysis shows that E_∞ has the strongest influence on the model's fit, followed by the arms with the higher time constants in succession of time constant.